Production of Nickel-Rich Cathodes for Lithium-Ion Batteries from Lab to Pilot Scale under Investigation of the Process Atmosphere

Carina A. Heck,* Fabienne Huttner, Julian K. Mayer, Olga Fromm, Markus Börner, Thilo Heckmann, Philip Scharfer, Wilhelm Schabel, Martin Winter, and Arno Kwade

The selection of an appropriate cathode active material is important for operation performance and production of high-performance lithium-ion batteries. Promising candidates are nickel-rich layered oxides like $LiNi_xCo_yMn_zO_2$ (NCM, x+y+z=1) with nickel contents of 'x' $\geq$ 0.8, characterized by high electrode potential and specific capacity. However, these materials are associated with capacity fading due to their high sensitivity to moisture. Herein, two different polycrystalline NCM materials with nickel contents of $0.81 \leq$ 'x' ≤ 0.83 and protective surface coatings are processed in dry-room atmosphere (dew point of supply air $T_D \approx -65\,°C$) at lab scale including the slurry preparation and coating procedure. In comparison, cathodes are produced in ambient atmosphere and both variants are tested in coin cells. Moreover, processing at pilot scale in ambient atmosphere is realized successfully by continuous coating and drying of the cathodes. Relevant electrode properties such as adhesion strength, specific electrical resistance, and pore-size distribution for the individual process steps are determined, as well as the moisture uptake during calendering. Furthermore, rate capability and cycling stability are investigated in pouch cells, wherein initial specific discharge capacities of up to 190 mAh g^{-1} (with regard to the cathode material mass) are achieved at 0.2C.

1. Introduction

Next to olivines (e.g., $LiFePO_4$) and spinel types (e.g., $LiMn_2O_4$), especially layered oxides such as $LiNi_xCo_yMn_zO_2$ (NCM, x+y+z =1) are commonly used as cathode active material.[1] One strategy to improve the specific capacity of NCM active materials is to increase the nickel (Ni) content. However, a high-delithiation degree at elevated potentials is associated with a lower structural stability of the Ni-rich NCM materials, resulting in severe capacity fading.[2] In this context, Laszczynski et al.[3] report an increased impedance of the cathode associated with an increased evolution of O_2, H_2, and CO_2, as well as stronger Ni dissolution for a cutoff voltage of 4.6 V for graphite/$LiNi_{0.8}Co_{0.1}Mn_{0.1}O_2$ (NCM811) cells. Furthermore, the higher Ni content results in a higher alkalinity of the active material and thus in a stronger adsorption of atmospheric water.[4] Interactions of the active material with water (H_2O) and carbon dioxide (CO_2) lead to the formation of decomposition products, such as lithium carbonate (Li_2CO_3) or lithium hydroxide (LiOH).[5] Apart from this, reaction with H_2O and CO_2 can also result in the formation of transition-metal hydroxides and carbonates on the material surface.[6] Consequently, these products can affect the slurry viscosity, material degradation, and gassing formation behavior.[5,7] Therein, Busà et al.[8] reported phase transformations and structural changes in the particles, resulting in higher impedance and capacity loss for NCM811 materials stored at ambient atmosphere. In this context, Wu et al.[9] revealed the role of the impurity phase at the surface of Ni-rich cathode active material. Here, an irreversible phase transition from the surface to bulk in Ni-rich cathodes is triggered by the intermediate disordered cation mixing domain instead of the pure rock-salt phase, resulting in capacity fading, structural degradation, and

C. A. Heck, F. Huttner, J. K. Mayer, A. Kwade
Institute for Particle Technology
Technische Universität Braunschweig
38104 Braunschweig, Germany
E-mail: c.heck@tu-braunschweig.de

The ORCID identification number(s) for the author(s) of this article can be found under https://doi.org/10.1002/ente.202200945.

C. A. Heck, F. Huttner, J. K. Mayer, A. Kwade
Battery LabFactory Braunschweig
Technische Universität Braunschweig
38106 Braunschweig, Germany

O. Fromm, M. Börner, M. Winter
MEET Battery Research Center
University of Münster
48149 Münster, Germany

T. Heckmann, P. Scharfer, W. Schabel
Thin Film Technology
Karlsruhe Institute of Technology
76131 Karlsruhe, Germany

thermal instability.[9] Thus, the NCM material is structurally modified during processing by atmosphere contact. Faenza et al.[10] demonstrated good long-term performance of lithium nickel–cobalt–aluminum oxide (NCA)-based cathodes by retaining Li_2CO_3 on the particle surface while removing byproducts like $LiHCO_3$, H_2O, and LiOH. Nevertheless, it is still necessary to avoid the formation of these substances. Therefore, several solutions at material level were developed to reduce the negative effects on the electrode performance. Possibilities to improve the active material properties are the application of an appropriate surface coating, "doping" with foreign elements, or the introduction of a core–shell or gradient structure.[5,7,11–13]

In general, H_2O is considered as a critical impurity in lithium-ion batteries (LIBs). It can adversely affect the cathode performance and react with the commonly used conducting salt, $LiPF_6$.[14,15] This reaction results in amongst others the formation of hydrofluoric acid (HF), which is presumably mostly dissolved to form additional acidic decay products.[16] Among others, the reaction products have a detrimental effect on the cell resistance. As a consequence, performance as well as safety properties of the battery are deteriorated.[14,16–19]

In this context, for commercialized $LiNi_{0.6}Co_{0.2}Mn_{0.2}O_2$ (NCM622) cathodes, it was shown that a stable cell performance can be achieved by an appropriate post-drying strategy of the electrodes. The post-drying step is most commonly conducted prior to cell assembly and aims to reduce the total cell moisture amount below a critical level.[14,19] Interestingly, in a previous study with single-compartment pouch cells (graphitic anode/ NCM622-based cathode), the cells post-dried with the mildest post-drying procedure achieved the best electrochemical performance despite having the highest residual moisture content.[14] In this study, it was shown that high post-drying intensities can damage the sensitive binder network of the electrodes and that a certain level of residual moisture does not impair the electrochemical performance. In this context, small amounts of water within the battery cell can also have some advantageous effects: Langklotz et al.[18] reported that a diffusion of water molecules from the cathode side through the battery cell can influence both electrodes. For instance, a low moisture content supports the formation of an effective solid electrolyte interphase (SEI) on the anode. An effective SEI can protect the anode against decomposition by the electrolyte at low potentials, which results in a more stable electrochemical performance.[20] This illustrates the complex influence of moisture within the battery cell.

Only a few studies investigated the impact of the process atmosphere on cell performance of Ni-rich NCM-based cathodes. In one study, NCM811 powder, which was excessively exposed to moisture, was compared to dried and calcined NCM811 with regard to electrochemical properties.[6] The best performance was obtained for the calcined material with a capacity retention of 92% after 250 cycles at 1C compared to 85% for the dried material and 55% for the weathered material. In addition, the authors questioned the detrimental effect of Li_2CO_3, but considered Ni carbonate ($NiCO_3$) as the most significant surface contaminant.[6] Moreover, former investigations conducted at lab scale for Ni-rich cathodes processed in ambient atmosphere demonstrated that a good performance is achievable by a short retention time in ambient atmosphere and an appropriate post-drying procedure.[21] However, information is given rarely with

regard to production of Ni-rich cathodes at larger scale, enabling a continuous processing. For NCM cathodes with lower Ni content, continuous coating and drying are already well established.[22–25] For Ni-rich NCM, the production at industrial scale with a batch approach in nitrogen atmosphere and manufacturing of double-side electrodes were reported.[26] Nonetheless, further investigations are highly relevant for Ni-rich cathode production to enable processing of Ni-rich active materials like $LiNi_{0.9}Co_{0.05}Mn_{0.05}O_2$ at industrial scale.[27]

In a former study,[21] cathodes based on pretreated (coated/ doped) Ni-rich NCM were produced at lab scale within ambient atmosphere and analyzed with regard to moisture content and structural properties. Before cell assembly, two post-drying procedures were applied which differed in their intensity. The electrochemical performance was tested in half coin cells and compared to cells built of cathodes produced in dry-room atmosphere. The results showed that the production of Ni-rich NCM based cathodes seems to be possible at ambient atmosphere, if the NCM is pretreated and adequate post-drying is applied. The more intense procedure (4 h under vacuum with 0.5 h argon purging at 80 °C) resulted in a higher specific discharge capacity, which is why a comparable post-drying strategy was selected for the current study.

The current work focusses on the investigation of the influence of the process atmosphere, as well as the establishment of a pilot scale process route for Ni-rich NCM-based cathodes. Here, coated NCM materials were selected to verify the impact of process atmosphere when a protective surface layer is used. First, the impact of atmosphere, so processing in a dry room versus processing in ambient environment, on the electrochemical performance of two polycrystalline Ni-rich NCM-based cathodes, was investigated at lab scale. Based on these results and the findings of the former study,[21] pilot-scale production was then realized in ambient atmosphere. Cathodes with the coated polycrystalline NCM materials with different particle sizes from different suppliers were produced in pilot scale and continuously coated and dried in ambient process atmosphere. For individual process steps, the relevant electrode properties like adhesion strength, electrical resistance, porosity, and moisture content were determined. Furthermore, C-rate testing and long-term cycling were conducted for single-compartment pouch cells.

2. Lab-Scale Results—Atmospheric Impact on Cell Performance

Figure 1 illustrates the specific discharge capacity of coin cells (two-electrode configuration[28]) with calendered polycrystalline Ni-rich active material–based cathodes against lithium-metal anodes. The cathode slurry was produced and coated in ambient (dew point $T_D \approx 0$ °C) or dry-room atmosphere ($T_D \approx -65$ °C of supply air) at lab scale. Calendering was performed in ambient atmosphere. The initial specific discharge capacities for the third formation step at 0.05C are shown in **Table 1**. It should be noted that processing of the cathodes in dry-room atmosphere leads to a similar (Ni-rich_polyB) or slightly higher specific discharge capacity (approx. 2.4% higher for Ni-rich_polyA at 0.05C) in comparison to cathodes processed in ambient atmosphere. For Ni-rich_polyA, the cathodes produced in dry-room
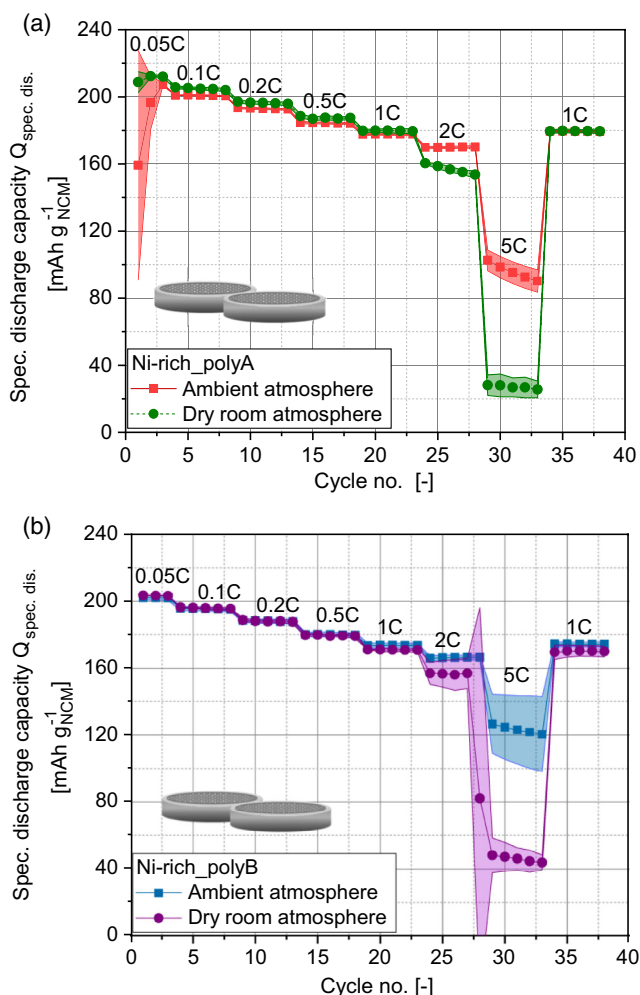
Figure 1. Specific discharge capacity of lithium metal/NCM coin cells. a) Ni-rich_polyA cathodes and b) Ni-rich_polyB cathodes produced in ambient or dry-room atmosphere.

Table 1. Initial specific discharge capacities obtained from third formation step (0.05C).

Cathode active material	Ambient atmosphere processing [mAh g^{-1}]	Dry-room processing [mAh g^{-1}]
Ni-rich_polyA	207	212
Ni-rich_polyB	202	203

atmosphere show slightly higher specific discharge capacities for C-rates up to 1C. Remarkably, at higher C-rates, cells based on cathodes produced in ambient atmosphere show a superior performance. Moreover, for Ni–rich_polyB cathodes, beyond the similarity in specific discharge capacities for C-rates up to 0.5C, cathodes processed in ambient atmosphere also exhibit a superior electrochemical performance at higher C-rates. These results are in contrast to the expected effects due to high sensitivity of Ni-rich NCM material to moisture.[4,7] Wu et al.[4] reported an improved capacity retention of 5% after 50 cycles at

1C for an NCM811 slurry produced in dry atmosphere (5% relative humidity) in comparison to processing at room temperature and room humidity. However, they confirm very recent results of Mayer and Huttner et al.[21] One reason might be the use of protective coatings on the pristine material surfaces, applied by the manufacturers to prevent degradation at high-delithiation degrees or in presence of moisture.

The results demonstrated that a reduction of moisture content to an attainable minimum does not gain much higher specific capacities and, thus, might not be necessary especially from an ecological and economic view. Therefore, it was concluded that further studies are needed to determine an optimal process atmosphere at higher dew points between $T_D = -65$ and 0 °C. Moreover, the atmospheric impact on electrochemical performance must be evaluated for long-term cycling. Very low dew points ($T_D = -65$ °C) do not seem to be required to achieve good performances, meaning higher costs during cathode processing can be avoided. In addition, the results of a previous study suggest that different process atmospheres cause varying process conditions to occur already during mixing and dispersing stage.[21] Thus, the particles in the slurry experience slightly different mechanical stresses, which leads to deviations in the resulting electrode microstructure. For example, lower particle sizes of carbon black (CB) agglomerates, due to higher mechanical stresses, lead to a decrease of inner CB domain porosity, which can subsequently affect the C-rate capability. The resulting trend corresponds to an optimum curve.[29] Results from several studies demonstrate that with this material system and process conditions, the CB agglomerate size should be comparatively low. Therefore, a reduction in CB agglomerate particle size is assumed to ultimately result in a deterioration of the C-rate capability beyond a certain threshold. Under dry-room conditions, the viscosity is generally higher than in ambient atmosphere due to a stronger solvent evaporation. This can result in more mechanical stress on the particles during dispersion. Therefore, a lower CB porosity occurs, which leads to lower capacity yields at higher C-ratios. Due to these predicted differences in electrode microstructure, variations in overall ionic conductivity and thus C-rate capability, are to be expected for different processing atmospheres.[30] However, because calendering was performed in ambient atmosphere, future research should address the investigation of a process route fully implemented in dry-room atmosphere at different dew points, especially due to an increased water uptake of the cathodes caused by calendering (see **Figure 2**). Nevertheless, the result of a similar or even better performance of Ni-rich cathodes with coated active material processed in ambient atmosphere meaning a higher retention time in a more humid environment is of high importance because it could lead to a significant reduction of process costs.[31]

3. Pilot-Scale Results—Cathode Production at Ambient Atmosphere

To verify the results obtained at lab scale that good performance is possible at ambient process atmosphere, a production at pilot scale for both polycrystalline NCM materials was conducted in ambient atmosphere. Herein, the cathode slurries were coated continuously onto an aluminum substrate current collector.
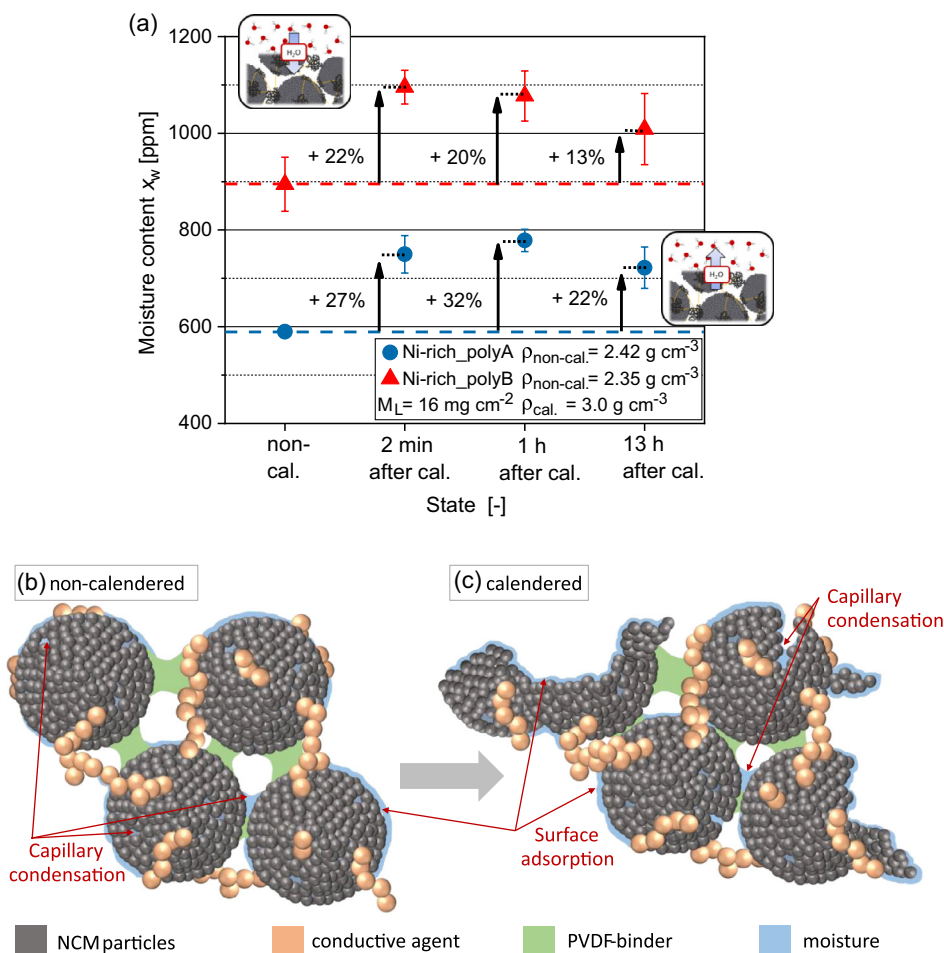
Figure 2. Top: a) moisture content of the Ni-rich_polyA and Ni-rich_polyB cathodes before and after calendering (cal.) determined by Karl–Fischer Titration. Bottom: schematic illustration of water adsorption in an NCM-based cathode in b) non-calendered and c) calendered state (Adapted by permission from Ref. [32], Copyright (2021) IOP Publishing, CC BY 4.0).

The entire process chain from dry premixing up to calendering was performed in ambient atmosphere with a dew point of $T_D \approx 0\,°C$. To investigate the water (de-)adsorption behavior of the cathodes along the process chain, the moisture of the cathodes was determined by Karl–Fischer Titration (KFT) after coating and drying, that is, in the non-calendered state (non-cal.), as well as after calendering (after cal.) (cf. Figure 2a). In previous studies with cathodes based on polycrystalline NCM622, Huttner et al.[32] showed that cathodes adsorb more water after calendering, due to an increased surface area caused by cracking within the secondary particle structure induced by calendering, as well as particle breakage. A schematic illustration of this is presented in Figure 2b,c. Mayer and Huttner et al.[21] observed the same phenomenon for cathodes containing different polycrystalline Ni-rich NCM active materials. Hence, a higher moisture uptake of the cathodes after calendering was expected in the current study as well. To investigate this phenomenon in detail, samples for moisture measurements of the cathodes were taken of the cathodes directly (2 min), 1 h, and the next day (13 h) after calendering in ambient atmosphere. The results are shown in Figure 2a.

In general, the Ni-rich_polyB-based cathode contains on average 43% more moisture in comparison to the Ni-rich_polyA-based cathode. According to scanning electron microscopy (SEM) analysis (see Figure 5), this might result from a higher surface area of the Ni-rich_polyB cathode, due to a smaller particle size and a higher amount of primary particles already before calendering. Furthermore, the calculation of the porosities of the conductive network, ε_{CN}, shows that Ni-rich_polyA (22.5%) has lower values than Ni-rich_polyB (27.7%). This trend agrees with the results of Mayer and Huttner et al.,[21] according to which a certain amount of the increased water uptake after calendering was attributed to an increased amount of pores in the electrode microstructure. After calendering, both cathodes show the expected water uptake. The Ni-rich_polyA cathode contains 27% and the Ni-rich_polyB cathode contains 22% more moisture in the compressed state. The measurements performed 1 and 13 h after calendering show that this water uptake is a permanent effect, as the moisture values remain at a high level for Ni-rich_polyA and Ni-rich_polyB cathodes, but depends on the surrounding atmosphere. The slight moisture loss after 13 h of exposure to ambient atmosphere can be traced back to drier

atmosphere in the laboratory during night, in absence of persons or conducted experiments. As a verification of the moisture content determination via KFT, sorption equilibria of the Ni-rich cathodes were measured by means of the magnetic suspension balance. This experimental setup controls the relative humidity in a measurement cell and weighs the sample mass while incrementally increasing the relative humidity after an equilibrium was reached. The results are plotted in **Figure 3**. For reference, the dashed line marks the equivalent of the dew point ($T_D = 0\,°C$) in relative humidity. The water uptake of both materials increases with increasing relative humidity. The comparison of Ni-rich_polyA and Ni-rich_polyB confirms the observation of the KFT: Ni-rich_polyB sorbs more moisture compared to Ni-rich_polyA. The absolute value of the moisture uptake at $T_D = 0\,°C$ of the sorption measurement expresses an offset compared to the data of the KFT. Such an offset is expected for the complex adsorption behavior of Ni-rich cathode materials, where sorption and desorption isotherm are not equivalent. The difference in moisture content detection results from the different characteristics of the two measurement techniques. The KFT detects desorbed moisture at 120 °C, while the sorption measurement gravimetrically detects adsorbed moisture. Nevertheless, this circumstance affects both samples equally, which assures reliability of the results. The results confirm the previously stated theory that the higher water uptake of the Ni-rich_polyB can be attributed to the larger surface area, and consequently higher surface adsorption. The determined specific surface area of the Ni-rich_polyB cathode in the non-calendered state is $1.76\,m^2\,g^{-1}$, whereby it amounts only to $0.96\,m^2\,g^{-1}$ for the Ni-rich_polyA cathode.

In **Figure 4**, the pore-size distributions of the non-calendered and calendered cathodes are illustrated. First, the general porosities of the non-calendered electrodes are at similar levels: Ni-rich_polyA ($\varepsilon_{C,polyA} = 27.0\%$) is slightly lower than Ni-rich_polyB ($\varepsilon_{C,polyB} = 28.4\%$). Considering the pore-size distribution, Ni-rich_polyB cathodes have a smaller pore size in comparison to Ni–rich_polyA cathodes. This effect is due to the smaller-size active material particles, which can be confirmed by SEM analysis (**Figure 5**). More SEM images of
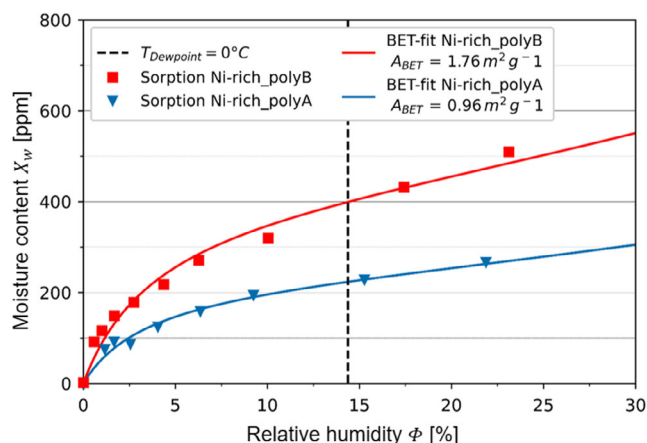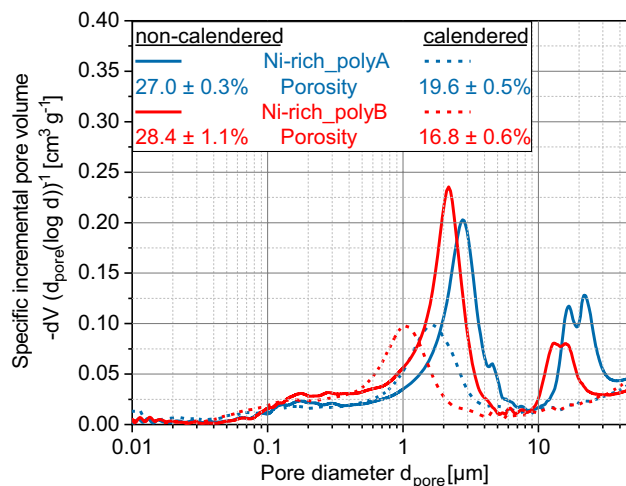

Figure 4. Pore-size distribution of the non-calendered and calendered Ni-rich_polyA and Ni–rich_polyB cathodes. Target coating density of the calendered cathodes: $\rho_C = 3.0\,g\,cm^{-3}$.

the non-calendered and calendered state for both materials are provided in the Supporting Information. Furthermore, Ni-rich_polyB already shows primary particles in the non-calendered state, while the raw material does not show particle breakage (not shown here). This means that already during dispersing, the shear stresses transmitted by the fluid are sufficient to fragment the active material particles. After calendering, the degree of particle breakage further increases, resulting in a denser electrode structure. This is represented by a slightly lower porosity ($\varepsilon_{C,polyB} = 16.8\%$) and smaller pore size on average, in comparison to Ni-rich_polyA ($\varepsilon_{C,polyA} = 19.6\%$).

Figure 6 demonstrates the specific electrical resistance of the cathodes in non-calendered, calendered, and post-dried state determined according to Westphal et al.[33] by using a direct current (DC) source. Resistance data can help to understand the formed microstructure and resulting electron-transport characteristics.[33] The resistance of Ni-rich_polyB cathodes is significantly higher in the non-calendered state. In this cathode, the active material particles already have numerous fractures in the non-calendered state (see Figure 5), and thus a correspondingly higher surface area that needs to be contacted by the CB/binder (CB/B) network. Hence, the active material particles are connected more weakly, and a lower electrical connectivity between the particles is reached in comparison to Ni-rich_polyA. After calendering, the resistance of both cathodes is reduced significantly. This can be assigned to better electrical contact due to the formation of an increased number of contact points within the conductive network and between the conductive network and the active material particles.[34] After post-drying, the electrical resistance further increases for Ni-rich_polyB cathodes. In this regard, previous studies proposed thermally activated binder creeping during post-drying, leading to a certain degradation of the whole microstructure.[14] Therefore, it was concluded that the lower binder volume/surface area ratio of the Ni-rich_polyB cathode resulted in very thin and fragile binder/CB connections. The fragile connections

Figure 3. Sorption isotherms of Ni-rich_polyA and Ni-rich_polyB cathodes in non-calendered state obtained from magnetic suspension microbalance measurements (30 °C).
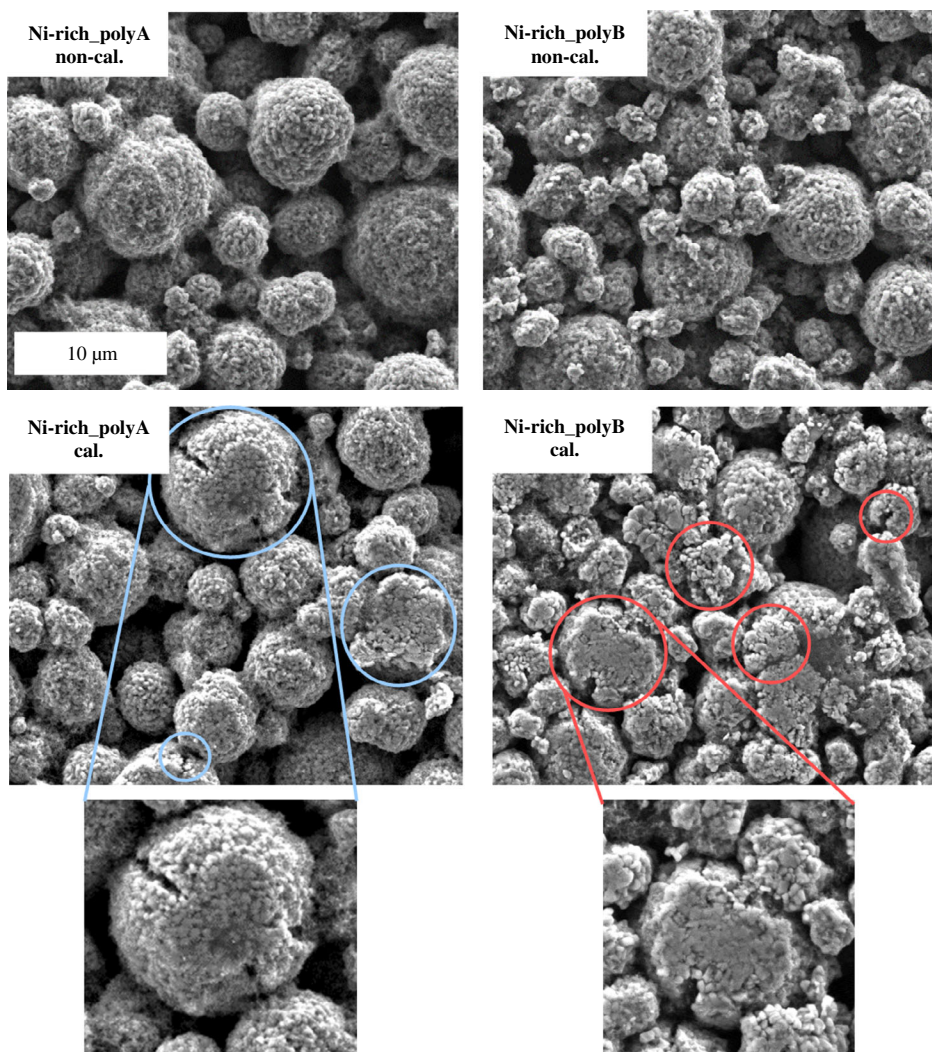
**ADVANCED
SCIENCE NEWS**

www.advancedsciencenews.com

Energy Technology
Generation, Conversion, Storage, Distribution

www.entechnol.de

Figure 5. Scanning electron microscope (SEM) images of non-calendered and calendered Ni-rich_polyA and Ni-rich_polyB cathodes with a magnification of 4400×. Examples of particle breakage and cracking are marked by cycles.

were potentially damaged during post-drying, resulting in an increase of electrical resistance.

Moreover, the adhesion strength of the cathodes in non-calendered, calendered, and post-dried state was measured (Figure 6) according to Haselrieder et al.[35] The adhesion strength for both cathode variants decreases after calendering. This phenomenon is already described for low to medium strong calendering for cathodes based on NCM622,[32,36] and also Ni-rich NCM (Ni contents of >0.8).[21] Shear forces lead to contact losses within the structure. Essentially, the polyvinylidene fluoride (PVDF) binder is responsible for the cohesion between the particles and adhesion of the particles to the current collector due to mechanical interlocking mechanisms and interfacial forces, such as a dipole and weak Van der Waals forces.[32,37]

During compression, these interfacial forces can be damaged by shear and tensile stresses and consequently the contact points of binder and current collector are separated.[32,36,38] Nevertheless, after post-drying at 80 °C under vacuum, a higher adhesion can be achieved. This is probably due to the

aforementioned thermally induced binder creeping of the thermoplastic PVDF, whereby contact points between the particles and current collector are rebuilt, enhancing the adhesion strength.[14,32] Based on previous investigations, an intensive post-drying procedure under vacuum for 5 h and periodical argon flushing was performed before cell assembly.[21] To evaluate the impact of processing at ambient atmosphere on the cell quality, full-pouch cells were built, using a graphite anode and a Separion separator. In **Figure 7**, the resulting total cell moisture is displayed, calculated according to the mass ratios of the cell components in each cell without current collectors. Post-drying reduces the water content of the Ni-rich_polyA-based cathode by 37% to 454 ppm and of the Ni-rich_polyB-based cathode by 34% to 665 ppm. Hence, due to its higher surface area, the Ni-rich_polyB not only contains more moisture in comparison to Ni-rich_polyA before and after calendering (see Figure 2), but also after post-drying. The mass ratio in the Ni-rich_polyA cells is 45:19:36 (cathode:separator:anode), while in the Ni-rich_polyB cells is 44:20:36. Due to the higher moisture content of the
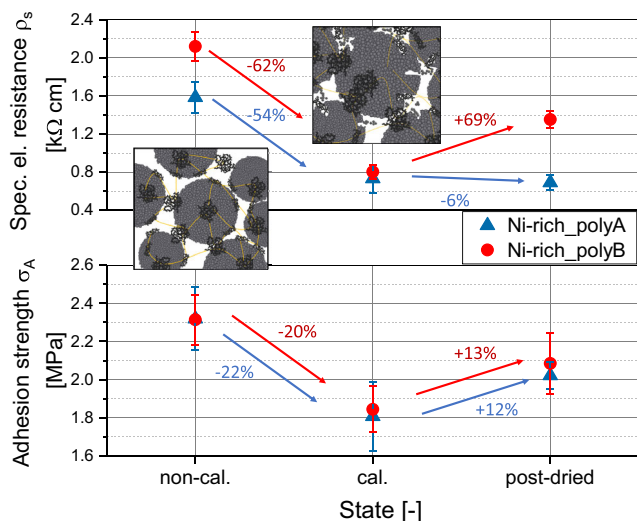
Figure 6. Specific electrical resistance and adhesion strength at different process steps of the Ni-rich cathodes.

Figure 8. C-rate testing of lithium-ion battery (LIB) graphite/NCM pouch cells with Ni-rich_polyA and Ni-rich_polyB cathodes. Charging rate was set to 0.2C.

cathode after post-drying, the Ni-rich_polyB cells contain 21% more moisture (534 ppm) compared to the Ni-rich_polyA cells (441 ppm).

In **Figure 8**, the specific discharge capacity during C-rate testing of one compartment pouch cells is shown. In correlation to the results of the two-electrode lithium-metal/NCM coin cells (cf. Figure 1), graphite/NCM pouch cells with Ni-rich_polyA show higher discharge capacities in comparison to those with Ni-rich_polyB during C-rate testing. In the third formation step (0.2C/0.2C) after initial capacity increase,[39] the Ni-rich_polyA cells reach an initial discharge capacity of 190.3 mAh g^{-1}, whereas the Ni-rich_polyB cells only achieve 178.8 mAh g^{-1}. Reasons for the differing electrochemical performance of the Ni-rich_polyA and Ni-rich_polyB cathodes can be attributed to the different particle sizes of the two active materials used, which result in different microstructures of the composite cathode,
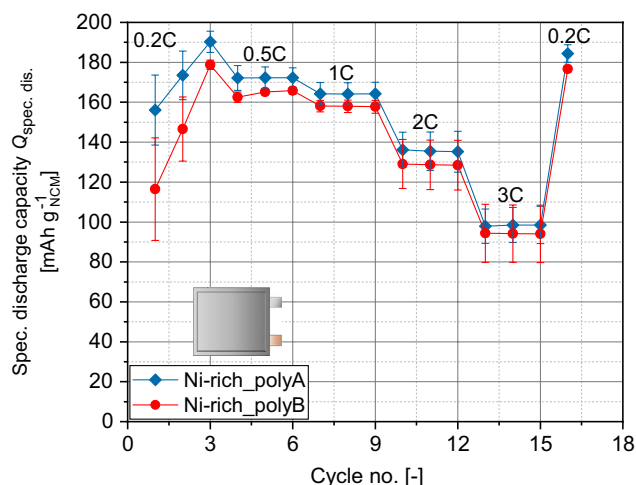
affecting the electron- and lithium-ion transportation, as well as the use of different surface coatings protecting the active material from atmosphere impacts. In addition, the higher cell moisture and the higher moisture in the cathode can affect the electrochemical performance of the Ni-rich_polyB. Due to the higher moisture, the formation of thick and resistive interphases between the electrodes and the electrolyte, namely cathode electrolyte interphase (CEI[40]) and SEI, could have been promoted.

Reaction of moisture with the conducting salt could have initiated cell capacity degradation.[14,15] In **Figure 9**, the specific differential capacity versus voltage curves for both cathode variants during the C-rate testing at different C-rates are shown. For each C-rate, the third charge and related discharge cycle step were analyzed. For both cathode materials, one cells was analyzed. In principle, four redox peaks can be identified within the charge curves, attributed to the phase transition in the
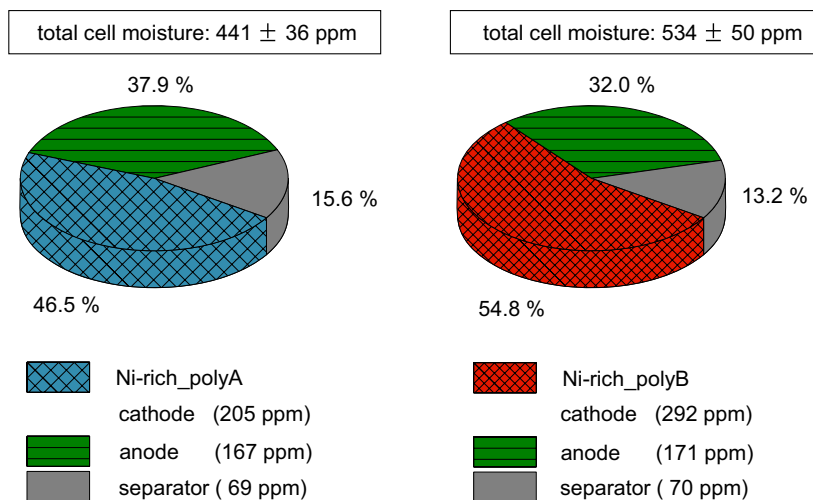

Figure 7. Total cell moisture of the single-compartment pouch cells after post-drying, with indication of the moisture amounts of each cell component, calculated according to the mass ratios of the cell components without current collectors.
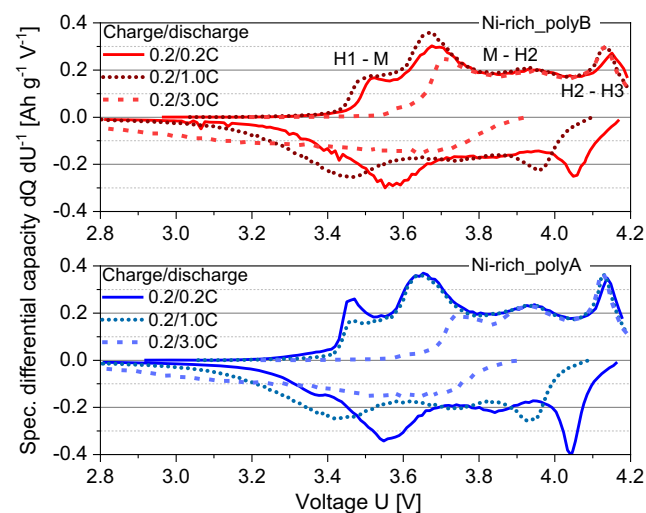
ADVANCED
SCIENCE NEWS
www.advancedsciencenews.com

Energy Technology
Generation, Conversion, Storage, Distribution

www.entechnol.de

Figure 9. Specific differential charge and discharge capacity versus voltage of Ni-rich_polyA and Ni-rich_polyB full-pouch cells at different C-rates during discharge (0.2C, 1C, 3C). For each C-rate, the third cycle is demonstrated.

Figure 10. C-rate testing and long-term cycling (1.0C/1.0C charge/discharge) of graphite/NCM pouch cells with the Ni-rich_polyA cathode.

NCM active material. This transition is induced by the de-/lithiation and a change in the oxidation state.[21,41] For the NCM material, the phase transition originally observed for LiNiO$_2$ is often applied, but probably was never verified for NCM itself.[42] However, to identify the phase transitions, the assignment proposed by Noh et al.[41] was applied herein.

The redox peaks shift with increasing C-rates and changes to a more polarized state, as described for other Ni-rich NCM active materials in similar studies.[21,41] Despite the higher discharge capacity of Ni-rich_polyA, the peak shift with increasing C-rate is comparable for both materials. This means that the capacity loss is equally pronounced for both materials with progressive C-rate testing. To be able to evaluate the long-term stability, long-term cycling was conducted on full-pouch cells with the better performing Ni-rich_polyA cathode.

Figure 10 illustrates the specific discharge capacity and capacity retention during long-term cycling at 1.0C. Cycling included 400 cycles, 16 cycles of C-rate testing, and 384 cycles at 1.0C/1.0C with a capacity retention of 93%.

These results illustrate the ability to achieve acceptable and stable cycling performance of Ni-rich NCM materials processed in ambient atmosphere at pilot scale when applying intense post-drying.[21] At the end, it is a question of costs and environment footprint if a somewhat better performance is reasonable by processing the electrodes in dry atmosphere. Slight capacity fading can be a result of electrolyte degradation and growth of the SEI, surface contaminations still remaining after processing, as well as the high-delithiation degree in the Ni-rich cathode and degradation of the anode active material.[2,7]

4. Conclusion

To evaluate the influence of the process atmosphere, two coated polycrystalline Ni-rich NCM materials were processed at lab scale
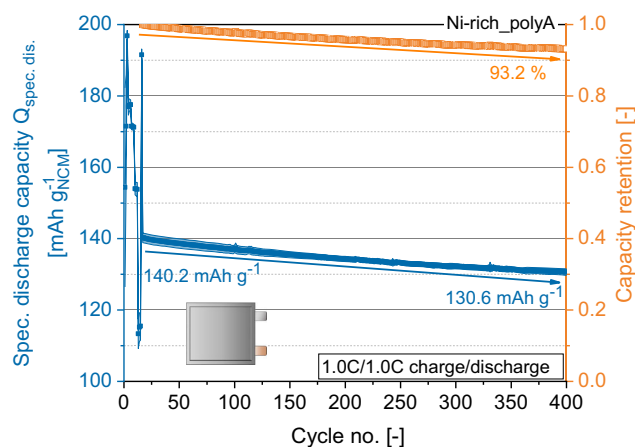
in ambient and dry-room atmosphere (dew point of the supply air $T_D \approx -65\,°C$) including the slurry preparation and coating procedure. Here, processing of Ni-rich cathodes in ambient atmosphere results in a similar or even better performance at high C-rates in comparison to cathode slurries produced and coated onto the current collector in a dry room. These findings are in contrast to the expectation found in literature due to the high sensitivity to moisture and probably result from the protective coating layer of the active material. However, they confirm results obtained in a former study.[21] As a next step, the polycrystalline Ni-rich NCM materials were processed within ambient atmosphere at pilot scale to verify good performance at a higher scale. Moreover, cathode properties were analyzed to obtain a deeper understanding of Ni-rich cathode production. The NCM materials showed differing moisture uptake behavior due to the different particle size, surface area, as well as possibly different surface material coatings. An enhanced moisture uptake after calendering was confirmed for both tested Ni-rich active materials as a result of particle breakage, leading to a higher surface area and smaller pore sizes. The electrochemical performance was finally investigated in single-layer full-pouch cells. An initial discharge capacity of up to 190 mAh g^{-1} at 0.2C was reached. This study shows that Ni-rich cathode production in ambient atmosphere is in principal possible when protective surface layers of the active material are used and should be at least considered when designing a cell production plant. Here, only short retention times in ambient atmosphere should be included, as well as a well-designed post-drying procedure.[21] The decision on the quality of process atmosphere depends on economic and ecological considerations as an ambient or only slightly dry atmosphere results in a significant reduction of process costs and environmental impact. Altogether, this study shows that Ni-rich cathode production at pilot scale is possible with production lines placed in rooms with ambient atmosphere. This provides the possibility of further using already existing production lines resulting in massive costs and energy savings. Requirements are protective surface layers on the raw material, adequate storage of raw materials and electrodes, and the application of a sufficient post-drying step before cell assembly.

In future, final assessment of the electrochemical performance of Ni-rich cathodes processed at ambient conditions should be performed in larger cells (capacity > 10 Ah) with a higher statistical relevant number. Moreover, processing with higher dew points than investigated in this study should be evaluated.

5. Experimental Section

Cathode Active Material: In this study, two different polycrystalline NCM cathode active materials with a Ni content 'x' between 0.81 and 0.83 from two different manufactures were investigated for cathode production (Ni-rich_polyA and Ni-rich_polyB). Both materials were coated by the manufacturers, but no further detail was given about the coating. Due to confidentiality agreements, no further information about the materials can be given.

Cathode Preparation at Lab Scale: Electrodes were prepared in different environments to exercise the influence of the process atmosphere on the electrochemical behavior of the NCM-based active materials. For this purpose, the electrode slurry was prepared on the following routes: mixing and coating procedure was either performed in ambient lab atmosphere or in a dry room with a dew point of the supply air of $T_D \approx -65\,°C$.

Electrode slurry was prepared using a composition of 95.5 wt% of the NCM-based active material, 1.5 wt% of PVDF as binder (Kynar Flex) and 3 wt% of conductive CB (C Energy Super C65, Imerys Graphite & Carbon), while aluminum foil (Speira GmbH) was used as current collector for the electrode. First, the binder polymer was dissolved in *N*-methl-2-pyrrolidon (NMP). Afterward, the appropriate amounts of conductive agent and active material were added and dispersed within 1 h with 8.4 m s^{-1} by utilizing a dissolver with toothed disc (ambient atmosphere: Dispermat LC30, VMA-Getzmann GmbH, dry-room atmosphere: Ultra Turrax, IKA-Werke GmbH & CO. KG) to especially disperse the CB particles. The electrode slurry was cast on the aluminum current collector by doctor blading (Zehntner GmbH) resulting in electrodes having an average active material mass loading of $M_L = 16$ to 18 mg cm^{-2}. The electrode sheets were dried for 1 h at 80 °C in a drying cabinet (Binder Labortechnik GmbH). Afterward, compression of the cathodes was performed by a calender (Guangzhou CLG electric Equipment Co., LTD). Then, electrode round punches with a diameter of 14 mm were cut out and the drying procedure was accomplished under reduced pressure of at least 10 mbar for 12 h at 100 °C (Büchi Labortechnik GmbH). The storage of the electrode punches and assembling of the coin cells were carried out in the dry room with a dew point of the supply air $T_D \approx -65\,°C$.

Cell Assembly and Electrochemical Behavior: Lab scale coin cells CR2032 with a two-electrode setup[28] were utilized for the electrochemical pre-investigations using high-purity lithium metal (Albemarle Corporation) as counter electrodes (CEs, Ø = 15 mm). The 1 M LiPF$_6$ in a mixture of ethylene carbonate (EC) and dimethyl carbonate (DMC) 1:1 by volume with 2 wt% of vinylene carbonate (VC) as additive was used as electrolyte. Round electrode punches as previously described were used as working electrodes (WE). In the evaluated system, a one-layer Whatman (Ø = 16 mm between WE and CE) was chosen as separator.

The NCM-based active materials were studied by C-rate tests in the potential range between 3.0 and 4.3 V versus Li/Li$^+$. The theoretical capacity of the cathode active materials was set to 200 mAh g^{-1}, thus, the specific current was set to 200 mA g^{-1} for a rate of 1.0 C. Corresponding to this calculation, the rate for the first 5 cycles at the beginning of C-rate test was set to 0.05 C (formation cycles to verify the capability of the active material). The following cycles were performed at 0.1C, 0.2C, 0.5C, 1.0C, 2.0C, and 5.0C and again 1.0C for five discharge cycles at each C-rate. The charging rate was chosen to be equal to the discharge rate for 0.05C, 0.1C, and 0.2C, for the higher discharge rates, it was set to be 0.2C. All experiments were performed in a climatic chamber at 20 °C using a Maccor Series 4000 automated test system (Maccor, Inc., USA). For electrochemical analysis, two cells were averaged.

Cathode Preparation at Pilot Scale: For processing at pilot scale, the polycrystalline active materials Ni-rich_polyA and Ni-rich_polyB were used.

The cathode slurries contained 95 wt% active material, 2 wt% CB (C Energy Super C65, Imerys Graphite & Carbon), and 3 wt% PVDF binder (5130, Solvay). NMP (BASF) was used as solvent. The dry compounds were mixed using a Turbula T2f (Willy A. Bachofen AG Maschinenfabrik) for 15 min and 49 min^{-1}. Afterward, the dry compounds were wet dispersed to a 600 mL batch with the solvent to a solids content of 70 wt%. For dispersion, a dissolver with tooth disc (Dispermat C60 VMA-Getzmann GmbH) was used. The procedure included 60 min of dispersing and a peripheral velocity of the disk of $\nu_p = 9$ m s^{-1}. Next, the slurry was coated using a continuous coating system with comma bar (Kroenert, LabCo) onto an aluminum current collector with a coating speed of $\upsilon_{CS} = 2$ m min^{-1}. The slurry was dried in a convective dryer with three stages of 2 m length ($\vartheta_{drying,1} = 60\,°C$, $\vartheta_{drying,2} = 80\,°C$, $\vartheta_{drying,3} = 100\,°C$, $t_{drying} = 3$ min) with a target mass loading of $M_L = 16$ mg cm^{-2} of the resulting cathode. Afterward, the cathodes were calendered to a target coating density of $\rho_C = 3.0$ g cm^{-3} by a Saueressig GKL 400 calender.

Cathode Characterization: Specific electrical resistance and adhesion strength were determined by a material testing machine (Z020, Zwick Roell GmBH). The measurement of the specific electrical resistance was performed according to Westphal et al.[33] and the measurement of adhesion strength according to Haselrieder et al.[35] Measurement was conducted for eight to ten cathode samples and averaged. To get reliable results, the device was placed in a dry room (dew point $T_D \approx -30\,°C$). Porosity and pore-size measurements were performed by mercury intrusion using a PoreMaster 60 (Quantachrome Instruments) according to Froboese et al.[43] The porosity of the conductive network ε_{CN} was determined by Equation (1) according to Mayer et al.[29] This evaluation considered the internal porosity of CB and the impact of the binder in terms of the cathode microstructure and, thus, expressed the porosity of the conductive network ε_{CN} (assumption: $\varepsilon_{CN} \approx \varepsilon_{CB}$).[21,29] The calculation of ε_{CN} included ε_C as the porosity of the coating, $\varepsilon_{C,AM}$ as the coating porosity resulting from the active material, as well as $c_{v,AM}$ as the volume fraction of the active material of the coating. Porosity data generated by mercury intrusion analysis were calculated with 0.01, 0.41, and 10 μm as lower, minimum, and upper pore-size limit. For estimation of the porosity, the mass loading of the cathodes was used.

$$\varepsilon_{CN} = \frac{\varepsilon_C - \varepsilon_{C,AM}}{1 - c_{v,AM} - \varepsilon_{C,AM}} \tag{1}$$

Determination of Moisture Content via KFT: The moisture content of the cathodes and anodes was determined according to Huttner et al.[14] by coulometric KFT, using an Aqua 40.0 titrator with headspace module (ECH Elektrochemie Halle). The titrator was placed in a dry room with a dew point of $T_D \approx -30\,°C$ to achieve reliable measurements. The cathodes were measured at 120 °C for 20 min, the anodes used for cell assembly at 100 °C for 10 min and the separators at 80 °C for 20 min. For each analysis, a threefold measurement was performed and averaged. For the status "13 h after calendering" of the Ni-rich_polyA cathode, only two values could be averaged. Because the current collector foil contained only marginal amounts of water, the moisture content was calculated only in relation to the coating.[44]

Determination of Sorption Equilibria via Magnet Suspension Balance: A magnet suspension microbalance gravimetrically measured the water uptake of a sample kept in a conditioned (temperature, humidity) environment. A variation of the humidity at a constant temperature yielded a sorption isotherm. The microbalance had a resolution of up to 1 ppm (for a sample weight of 10 g). The sample inside the measurement cell connected contactless via a magnetic suspension to the microbalance and was screened form the ambiance. A nitrogen flow saturated with water mixed with a dry nitrogen flow ($T_D < -65\,°C$) conditioned the measurement cell at ambient pressure. The precise activity (or relative humidity in case of water) of the sample was monitored via a chilled-mirror hygrometer at the exit of the measurement cell. This set up enabled the determination of sorption equilibria in the activity range of 0.0–0.3 and was employed in amble studies.[32,45–47] A commonly used equation to model sorption phenomena of is the Brunauer–Emmett–Teller (BET)

isotherm.[48] This equation accounted for multilayer adsorption onto the surface of a material and covered low activity ranges. The BET equation is given as follows

$$X = \frac{X_m \cdot k_{BET} \cdot a}{(1-a) \cdot (1 + (k_{BET} - 1) \cdot a)} \tag{2}$$

X and a are the solvent loading on the sample and sample's activity, respectively. k_{BET} and X_m are adjustable parameters to fit the isotherm to experimental data. The monolayer loading X_m provides further information about the surface area of the sample

$$A_{BET} = X_m \cdot A_i \cdot \frac{N_A}{\tilde{M}_i} \tag{3}$$

The surface area A_{BET} of the sample can be calculated with the Avogadro constant N_A, the molar mass $\tilde{M}_i$ of the adsorbing component, and the surface area required by an adsorbing molecule.[48] In case of water, this area is $12.5\,\text{Å}^2$.[48]

SEM Images: For visual analysis, an SEM from Thermo Fisher Scientific Inc. (Phenom XL) with a resolution of <14 nm at a primary beam voltage of 30 kV was used. One sample at a time was acquired at 10 kV with a resolution of 2048 × 2048 at 0.1 Pa in the sample chamber.

Post-Drying, Cell Assembly, and Electrochemical Characterization: One compartment two-electrode pouch cell assembly was realized in an argon-filled glove box (GS Glovebox Systemtechnik GmbH). For post-drying, anodes and cathodes were evacuated within the glove box oven under vacuum of 10^{-4} mbar for 5 h. After 1 h of heating up to 80 °C, every 30 min, a purging with argon gas was performed (up to 500 mbar).[21] Anodes with 93 wt% graphite as active material were used. Separion (Litarion GmbH) served as separator. As electrolyte, LP 57 (Gotion Inc.) containing 1 mol LiPF$_6$ and 2 vol% vinylene carbonate (VC) in a 1:1 mixture of EC and DMC was used. Full cells were tested in a MACCOR battery cycler at 20 °C. Formation includes three steps at 0.2C charge and discharge followed by a C-rate test (0.2C/0.5C, 0.2C/1C, 0.2C/2C, 0.2C/3C charge/discharge; three cycles each). After short recovery (0.2C/0.2C charge/discharge), long-time cycling was performed at 1.0C/1.0C charge. For electrochemical analysis, performance of the best three cells out of five was averaged.

Supporting Information

Supporting Information is available from the Wiley Online Library or from the author.

Conflict of Interest

The authors declare no conflict of interest.

Data Availability Statement

The data that support the findings of this study are available from the corresponding author upon reasonable request.

Keywords

[1] A. Kwade, W. Haselrieder, R. Leithoff, A. Modlinger, F. Dietrich, K. Droeder, *Nat. Energy* **2018**, *3*, 290.
[2] J. Kasnatscheew, S. Röser, M. Börner, M. Winter, *ACS Appl. Energy Mater.* **2019**, *2*, 7733.
[3] N. Laszczynski, S. Solchenbach, H. A. Gasteiger, B. L. Lucht, *J. Electrochem. Soc.* **2019**, *166*, A1853.
[4] X. Wu, D. Ruan, S. Tan, M. Feng, B. Li, G. Hu, *Ionics* **2020**, *26*, 5427.
[5] S. S. Zhang, *Energy Storage Mater.* **2020**, *24*, 247.
[6] S. Sicklinger, M. Metzger, H. Beyer, D. Pritzl, H. A. Gasteiger, *J. Electrochem. Soc.* **2019**, *166*, A2322.
[7] C. A. Heck, M.-W. von Horstig, F. Huttner, J. K. Mayer, W. Haselrieder, A. Kwade, *J. Electrochem. Soc.* **2020**, *167*, 160521.
[8] C. Busà, M. Belekoukia, M. J. Loveridge, *Electrochim. Acta* **2021**, *366*, 137358.
[9] F. Wu, N. Liu, L. Chen, N. Li, J. Dong, Y. Lu, G. Tan, M. Xu, D. Cao, Y. Liu, Y. Chen, Y. Su, *J. Energy Chem.* **2021**, *62*, 351.
[10] N. V. Faenza, L. Bruce, Z. W. Lebens-Higgins, I. Plitz, N. Pereira, L. F. J. Piper, G. G. Amatucci, *J. Electrochem. Soc.* **2017**, *164*, A3727.
[11] W. Liu, P. Oh, X. Liu, M.-J. Lee, W. Cho, S. Chae, Y. Kim, J. Cho, *Angew. Chem. Int. Ed.* **2015**, *54*, 4440.
[12] Y. Xia, J. Zheng, C. Wang, M. Gu, *Nano Energy* **2018**, *49*, 434.
[13] C. M. Julien, A. Mauger, *Energies* **2020**, *13*, 6363.
[14] F. Huttner, W. Haselrieder, A. Kwade, *Energy Technol.* **2020**, *8*, 1900245.
[15] S. Wiemers-Meyer, S. Jeremias, M. Winter, S. Nowak, *Electrochim. Acta* **2016**, *222*, 1267.
[16] U. Heider, R. Oesten, M. Jungnitz, *J. Power Sources* **1999**, *81–82*, 119.
[17] T. Kawamura, A. Kimura, M. Egashira, S. Okada, J.-I. Yamaki, *J. Power Sources* **2002**, *104*, 260.
[18] U. Langklotz, M. Schneider, A. Michaelis, *J. Ceram. Sci. Technol.* **2013**, *04*, 69.
[19] F. Huttner, A. Marth, J. C. Eser, T. Heckmann, J. Mohacsi, J. K. Mayer, P. Scharfer, W. Schabel, A. Kwade, *Batteries Supercaps* **2021**, *8*, 1900245.
[20] M. B. Pinson, M. Z. Bazant, *J. Electrochem. Soc.* **2013**, *160*, A243.
[21] J. K. Mayer, F. Huttner, C. A. Heck, D. Steckermeier, M.-W. von Horstig, A. Kwade, *J. Electrochem. Soc.* **2022**, *169*, 60512.
[22] J. K. Mayer, L. Almar, E. Asylbekov, W. Haselrieder, A. Kwade, A. Weber, H. Nirschl, *Energy Technol.* **2020**, *8*, 1900161.
[23] H. Bockholt, W. Haselrieder, A. Kwade, *ECS Trans.* **2013**, *50*, 25.
[24] J.-H. Schunemann, H. Dreger, H. Bockholt, A. Kwade, *ECS Trans.* **2016**, *73*, 153.
[25] G. Lenze, H. Bockholt, C. Schilcher, L. Froböse, D. Jansen, U. Krewer, A. Kwade, *J. Electrochem. Soc.* **2018**, *165*, A314.
[26] M. Keppeler, S. Roessler, W. Braunwarth, *Energy Technol.* **2020**, *8*, 2000183.
[27] C. Xu, Q. Dai, L. Gaines, M. Hu, A. Tukker, B. Steubing, *Commun. Mater.* **2020**, *1*, 437.
[28] R. Nölle, K. Beltrop, F. Holtstiege, J. Kasnatscheew, T. Placke, M. Winter, *Mater. Today* **2020**, *32*, 131.
[29] J. K. Mayer, H. Bockholt, A. Kwade, *J. Power Sources* **2022**, *529*, 231259.
[30] N. Epstein, *Chem. Eng. Sci.* **1989**, *44*, 777.

[31] N. von Drachenfels, J. Husmann, U. Khalid, F. Cerdas, C. Herrmann, *Energy Technol.* **2022**, *4*, 2200673.

[32] F. Huttner, A. Diener, T. Heckmann, J. C. Eser, T. Abali, J. K. Mayer, P. Scharfer, W. Schabel, A. Kwade, *J. Electrochem. Soc.* **2021**, *168*, 090539.

[33] B. G. Westphal, N. Mainusch, C. Meyer, W. Haselrieder, M. Indrikova, P. Titscher, H. Bockholt, W. Viöl, A. Kwade, *J. Energy Storage* **2017**, *11*, 76.

[34] C. Sangrós Giménez, C. Schilde, L. Froböse, S. Ivanov, A. Kwade, *Energy Technol.* **2020**, *8*, 1900180.

[35] W. Haselrieder, B. Westphal, H. Bockholt, A. Diener, S. Höft, A. Kwade, *Int. J. Adhes. Adhes.* **2015**, *60*, 1.

[36] C. Meyer, M. Weyhe, W. Haselrieder, A. Kwade, *Energy Technol.* **2020**, *8*, 1900175.

[37] H. Chen, M. Ling, L. Hencz, H. Y. Ling, G. Li, Z. Lin, G. Liu, S. Zhang, *Chem. Rev.* **2018**, *118*, 8936.

[38] T. Günther, D. Schreiner, A. Metkar, C. Meyer, A. Kwade, G. Reinhart, *Energy Technol.* **2020**, *8*, 1900026.

[39] J. Guo, Y. Li, J. Meng, K. Pedersen, L. Gurevich, D.-I. Stroe, *J. Energy Chem.* **2022**, *74*, 34.

[40] D. R. Gallus, R. Wagner, S. Wiemers-Meyer, M. Winter, I. Cekic-Laskovic, *Electrochim.* **2015**, *184*, 410.

[41] H.-J. Noh, S. Youn, C. S. Yoon, Y.-K. Sun, *J. Power Sources* **2013**, *233*, 121.

[42] W. Li, J. Reimers, J. Dahn, *Solid State Ionics* **1993**, *67*, 123.

[43] L. Froboese, P. Titscher, B. Westphal, W. Haselrieder, A. Kwade, *Mater. Charact.* **2017**, *133*, 102.

[44] M. Stich, N. Pandey, A. Bund, *J. Power Sources* **2017**, *364*, 84.

[45] F. Thurner, M. Stietz, *Chem. Eng. Process. Process Intensif.* **1984**, *18*, 333.

[46] J. C. Eser, B. Deichmann, T. Wirsching, L. Merklein, M. Müller, P. Scharfer, W. Schabel, *Drying Technol.* **2022**, *40*, 1130.

[47] J. C. Eser, T. Wirsching, P. G. Weidler, A. Altvater, T. Börnhorst, J. Kumberg, G. Schöne, M. Müller, P. Scharfer, W. Schabel, *Energy Technol.* **2020**, *8*, 1801162.

[48] S. Brunauer, P. H. Emmett, E. Teller, *J. Am. Chem. Soc.* **1938**, *60*, 309.